Segregated nanocompartments containing therapeutic enzymes and imaging compounds within DNA-zipped polymersome clusters for advanced nanotheranostic platform

Claire E. Meyer[1,&], Juan Liu[1,&], Ioana Craciun[1], Dalin Wu[1], Hui Wang[2], Mingqi Xie[2], Martin Fussenegger[2], Cornelia G. Palivan[1,]*

[1]C. E. Meyer, Dr. J. Liu, Dr. I. Craciun, Dr. D. Wu, Prof. C. G. Palivan

Department of Chemistry, University of Basel, Mattenstrasse 24a, Basel-4002, Switzerland

E-mail: cornelia.palivan@unibas.ch

[2]Dr. H. Wang, Dr. M. Xie, Prof. M. Fussenegger

Department of Biosystems Science Engineering, ETHZ, Mattenstrasse 26, Basel-4058, Switzerland

Keywords: DNA-polymersome clusters, catalytic nanocompartments, imaging nanocompartments, nanotheranostics, dopamine

Nanotheranostics is an emerging field that aims to bring together nanoscale-engineered materials with biological systems to provide a combination of both therapeutic and diagnostic strategies. However, current theranostic nanoplatforms have serious limitations, mainly because there is often a mismatch between the physical properties of the selected nanomaterials and their ease of functionalization, loading ability or overall compatibility with bioactive molecules. Herein we propose a new type of nanotheranostic system based on

nanocompartment clusters composed of two different types of polymersomes linked together by DNA. Careful design and procedure optimization allowed us to obtain clusters segregating human Dopa decarboxylase (DDC) as the therapeutic enzyme and fluorescent probes for the detection unit in distinct but colocalized nanocompartments. The diagnostic compartment provides a twofold function: firstly, trackability via dye-loading as the imaging component, and secondly, the ability to attach the cluster construct to the surface of cells expressing scavenger receptors. The therapeutic compartment, loaded with active DDC and permeabilized with outer membrane protein F (OmpF), triggers the cellular expression of a secreted embryonic alkaline phosphatase (SEAP) reporter enzyme via production of bioactive dopamine and activation of dopaminergic receptor D1 (DRD1), which is implicated in atherosclerosis. This dual-functionality polymersome cluster architecture provides a novel type of two-compartment nanotheranostic platform that is expected to provide the basis of a new treatment strategy for atherosclerosis. This system is expected to expand versatility and diversify the types of utilizable active molecules, and thus by extension expand the breadth of attainable applications.

1. Introduction

Theranostic approaches provide improved medical solutions by associating therapy with diagnostics, thereby avoiding multi-step procedures and reducing delays in treatment, which may be particularly crucial in the case of rapidly evolving diseases. In particular, appropriately designed nanocarriers for nanotheranostics could offer advantages such as longer circulation time, passive accumulation in tumor sites due to the enhanced permeability and retention (EPR) effect, controllable release of the payload, and specific targeting by surface modification.[1–3] To date nanotheranostics are based on single-assembly architectures, containing both therapeutic and imaging compounds.[1,4] These nanotheranostic single assemblies consist of

inorganic nanoparticles, polymeric micelles and soft nanocompartments (liposomes, polymersomes, layer-by-layer (LBL) capsules). The advantage of inorganic nanoparticles (quantum dots, superparamagnetic iron oxide nanoparticles (SPION), high-contrast gadolinium oxide (Gd_2O_3) nanoparticles, gold nanoparticles and gold nanorods) is that they intrinsically serve as imaging agents due to their specific properties, such as high luminescence, high contrast and localized surface plasmon resonance.[1] Stable small-molecular-weight drugs covalently bound to quantum dots and inorganic nanoparticles (doxorubicin (DOX),[5,6] camptothecin (CPT),[7,8] paclitaxel (PTX),[9] and palatinate[10]), as well as therapeutic proteins conjugated to the surface of nanoparticles,[11] or forming super-assemblies with nanoparticles,[12] have been introduced as theranostic systems. However, the use of inorganic nanoparticles for theranostic applications has limitations due to potential toxicity as a result of low clearance and accumulation.[13] Polymeric micelles have also been used for the development of nanotheranostics, mostly as carrier systems for both poorly soluble drugs and hydrophobic inorganic nanoparticles that can be co-encapsulated within their core.[14] However, their advantage of possessing a hydrophobic core is also a limitation, in that it allows the delivery of only hydrophobic payloads, which restricts the possible classes of deliverable compounds and thus the applications of this system.

Soft nanocompartments (liposomes and polymersomes) are an appealing alternative for development of nanotheranostics because their architecture, consisting of an aqueous cavity surrounded by a layer with hydrophobic core, allows simultaneous loading of hydrophilic and hydrophobic molecules/nanostructures (small molecules, proteins, inorganic nanoparticles, DNAs, etc).[15–20] In particular, polymersomes based on amphiphilic block copolymers have advantages over lipidic compartments, such as increased mechanical stability and greater chemical versatility, which is useful to control membrane properties, such as stimuli-

responsiveness, and programmability.[21,22] Polymersomes have been used both for co-delivery of drugs and imaging agents[23,24] and for development of catalytic compartments that mediate specific reactions inside the lumen.[25–27] For example, polymersomes loaded with enzymes and equipped with channel porins in the membrane were used for continuous production of antibiotics,[28] mimicking natural organelles by simultaneous degradation of reactive oxygen species and generation of a fluorescent product *in vitro*[29] and *in vivo*.[30] However, to our knowledge, theranostic polymersomes simultaneously bearing sensitive agents, such as degradable enzymes, along with imaging compounds have not been reported yet. As co-encapsulation of sensitive enzymes with inorganic nanoparticles or other imaging agents can be detrimental to the enzyme, the use of only one compartment represents a drawback in development of efficient protein-based nanotheranostics.

Super-assemblies are an alternative approach to co-encapsulation, as they consist of a combination of separate nanocompartments carrying complementary functions. To date, such super-assemblies have mostly been developed using inorganic nanoparticles,[31] such as gold nanorod dimers with $NaGdF_4$ satellite nanoparticles for imaging-guided phototherapy[32] and drug-encapsulated nanoparticles assembled into satellite structures with gold nanoparticles for chemothermal therapy and tumor imaging.[33] As most of the super-assemblies are held together by weak noncovalent interactions, they have the disadvantage of being vulnerable to dissociation, especially in long-term circulation and under complex physiological conditions.[34,35] Other super-assemblies based on micelles and soft nanocompartments have not yet been much explored, though their architecture might be more appropriate in terms of hosting sensitive molecules, such as enzymes, proteins, or RNA.

Here, we introduce a theranostic strategy based on DNA-linked synthetic nanocompartments (polymersomes) forming sub-micrometer clusters that have dual

functionality- imaging and enzymatic activity- and interact specifically with cells (**Figure 1**). Polymersomes serve to protect the encapsulated compounds, especially sensitive ones like degradable enzymes, from harmful environmental factors, including proteolytic attack.[36] In our approach, DNA hybridization induces the formation of polymersome clusters that promote colocalization of separated local environments, allowing simultaneous encapsulation of molecules without sacrificing the encapsulation efficiency or the activity of the payloads. We previously reported that the size and architecture of DNA-linked polymersome clusters can be well controlled,[37] while single-stranded DNA (ssDNA) can be employed to attach them to scavenger receptor-expressing cells.[38] Here, we re-engineered such DNA-linked polymersome clusters by loading them with imaging and catalytic compounds to support theranostics. The therapeutic catalytic nanocompartments are loaded with the recombinant human enzyme Dopa decarboxylase (DDC), which converts L-Dopa to bioactive dopamine.[39] Dopamine is a key factor in atherosclerosis prevention,[40] regulating vascular dynamics by activation of dopaminergic receptor D1 (DRD1).[41–43] Atherosclerosis is characterized by plaque buildup in the arteries, restricting blood flow. It often has no symptoms until a life-threatening event such as a heart attack or stroke occurs, highlighting the need for early prevention and detection.[44] The imaging nanocompartment was paired with the therapeutic compartment, as the second component of the theranostic clusters, in order to provide a sensitive detection method for atherosclerotic lesions by attaching to inflammatory cells recruited to these locations.[45,46] In order to prototype and monitor the properties of the imaging compartment, we chose a fluorescent dye (DY-633) to model the encapsulation of small hydrophilic imaging agents within polymersomes.

The potency of the theranostic clusters was evaluated with the cell line HEK_{REWARD}, which is specifically engineered to express human dopamine receptor 1 (DRD1)[47] and thus is

able to respond to dopamine enzymatically produced in the catalytic nanocompartment. The therapeutic activity of the DNA-linked polymersome clusters was determined by evaluating the concentration of the reporter, human secreted embryonic alkaline phosphatase (SEAP), produced by HEK_{REWARD} cells in the presence of dopamine, while their imaging function was established by visualizing their localization and interaction with the cell surface.

The unique advantage of our DNA-linked polymersome clusters over other currently available theranostic systems resides in the segregated location of the imaging and catalytic compounds, which allows them to act independently, without interference that might compromise their specific functionality. As our strategy is based on a modular design, it should be straightforward to expand it from the example presented here to a variety of other medical applications, simply by changing the functional components within the segregated compartments, and then zipping them together in clusters.

2. Results and Discussion

2.1. Design of theranostic polymersome clusters

2.1.1. Development strategy of DNA-linked nanocompartment clusters

Theranostic clusters are formed by self-organization of two types of nanocompartments: the therapeutic polymeric compartment that contains the catalytically active species, and the imaging polymeric compartment that allows the detection and tracking of the whole clusters (Figure 1). DNA hybridization was used as the driving force to control the construction of nanocompartment clusters with sub-micrometer size.[37] The therapeutic compartment was functionalized with one type of ssDNA (ssDNAa), while the imaging compartment bears the complementary ssDNAb at its surface (see Table S1 for the details of ssDNA sequences). In

order to modulate the DNA attachment to the polymersomes, we also used variants of these ssDNA sequences (called spacer-ssDNAa and spacer-ssDNAb), which contain an additional noncomplementary DNA linker acting as a spacer between the surface of the polymersomes and the complementary DNA sequence. We compared clusters made with spacer-ssDNA and clusters hybridized with ssDNA, in order to select the most suitable approach to support efficient theranostic application.

We selected amphiphilic diblock copolymers poly(dimethylsiloxane)-*block*-poly(2-methyloxazoline), PDMS-PMOXA for formation of the nanocompartments, because copolymers with a PDMS hydrophobic domain and a PMOXA hydrophilic domain generate polymersomes with flexible membranes,[48] increased mechanical stability and low toxicity, both *in vitro* and *in vivo*.[30] Azide-functionalized poly(dimethylsiloxane)$_{22}$-*block*-poly(2-methyloxazoline)$_8$ (PDMS$_{22}$-PMOXA$_8$-OEG$_3$-N$_3$) (Figure S1) was used to form polymersomes with exposed azide functional groups that do not interfere with other biological processes, as they are bio-orthogonal[49] and promote the attachment of ssDNA. Conjugation was carried out through azide–alkyne cycloaddition (SPAAC) between dibenzocyclooctyne (DBCO) covalently attached to the ssDNA and the azide moieties on the diblock copolymers.[37] We specifically selected short polymer blocks to generate nanocompartments with thin but stable membranes, in order to permit functional insertion of membrane proteins to support the *in situ* enzymatic reaction of the catalytic nanocompartment.[48] Importantly, low-molecular-weight PDMS$_{22}$-PMOXA$_8$ block copolymer is expected to self-assemble rapidly into vesicles, shortening the process of polymersome formation. Indeed, our PDMS$_{22}$-PMOXA$_8$-OEG$_3$-N$_3$ is particularly efficient as it self-assemble into vesicles in less than 1 min when rehydrated in PBS at room temperature (Figure S2). The vesicular structure of the obtained self-assembled nanocompartments was confirmed by a combination of transmission electron microscopy

(TEM), dynamic light scattering (DLS) and static light scattering (SLS) (Figure S2). The size of the polymersomes was 175 ± 88 nm, and the R_g/R_h ratio of the hydrodynamic radius (R_h) to the radius of gyration (R_g) was 0.96, indicating a hollow spherical architecture. This ease of formation of polymersomes, combined with the swiftness of $PDMS_{22}$-$PMOXA_8$-OEG_3-N_3 copolymer formation, also enabled us to increase the initial concentration of copolymer to 10 mg/mL, resulting in a high number of polymersomes ($1.3*10^{12}$ vesicles/mL as determined by nanoparticle tracking analysis).

Our strategy to obtain DNA-linked polymersome clusters for theranostics is modular, being based on three steps: i) the formation of imaging nanocompartments, ii) the formation of catalytic nanocompartments able to produce a specific therapeutic compound, and iii) the functionalization of each type of nanocompartment with ssDNA and complementary ssDNA to induce self-organization leading to the formation of nanotheranostic clusters. This design strategy based on segregated locations of the therapeutic and imaging compounds allows the flexible control of each component in terms of type of payload and associated properties. The final cluster, coupling both nanocompartments, enables control and tracking of the bio-location of the nanotheranostic platform, as well as delivering the desired cell response.

2.1.2. Formation of the imaging nanocompartment

The imaging nanocompartment (Dye-Ncomp) consists of a polymersome loaded with fluorescent dye. We chose to encapsulate DY-633 into polymersomes as a model of the entrapment of small imaging probes in the cavity of the nanocompartments. Like most of the small hydrophilic molecules that have been used to develop imaging nanocompartments, DY-633 is chemically stable, so Dye-Ncomp was formed under normal conditions (room

temperature, overnight stirring) by self-assembly through film rehydration of the $PDMS_{22}$-$PMOXA_8$-OEG_3-N_3 polymer (**Figure 2**A). The resulting imaging nanocompartments have a hydrodynamic diameter D_H of 218 ± 86 nm as measured by dynamic light scattering (DLS), and their spherical shape was confirmed by transmission electron microscopy (TEM) (Figure S3A). As expected, encapsulation of the dye did not affect the self-assembly process, and the resultant imaging nanocompartments appeared similar to empty ones (Figure S3B). Based on these results with DY-633, the incorporation of other imaging components consisting of stable small hydrophilic molecules should be relatively straightforward. In contrast, the development of therapeutic catalytic compartments is more complex, as it involves active enzymes.

2.1.3. Formation of the catalytic nanocompartment with a therapeutic role

The catalytic nanocompartment (DDC-Ncomp) consists of human DDC encapsulated in the inner cavity of polymersomes equipped with a channel porin, which supports *in situ* enzymatic reactions by allowing the passage of substrates and products through the polymeric membrane (Figure 2B). Compared to other therapeutic nanocompartments reported for theranostic applications, which are based on the entrapment of small and stable therapeutic compounds,[1] we aimed to develop a more versatile and dynamic system involving an active enzyme that produces the desired drug inside the therapeutic compartment. By incorporating an active enzyme, we can produce the needed therapeutic compound on demand at selected locations rather than having a simple one-time delivery system. But, like many enzymes carrying out physiological functions in the human body, DDC is vulnerable to degradation, and loses its activity significantly at 37 °C.[50]

Therefore, the formation of DDC-Ncomp requires a complex preparation methodology based on numerous optimization steps, compared to regular encapsulation of small stable compounds

inside polymersomes. To preserve DDC activity, it was crucial to conduct polymersome formation as quickly as possible by shortening the time of film rehydration, since at least one day is generally required for the self-assembly of most amphiphilic block copolymers with high molecular weight.[29,51] Our short $PDMS_{22}$-$PMOXA_8$-OEG_3-N_3 copolymer favoured the formation of polymersomes in less than 1 min, thus supporting a rapid generation of DDC-Ncomps (see above). It was also essential to permeabilize the polymeric membrane of PDMS-PMOXA polymersomes to support enzymatic activity by implementing small-molecular flow through the nanocompartment. We chose the channel porin OmpF as a biological tool for permabilization, as it can be inserted in the membrane of PDMS-PMOXA polymersomes and has a molecular weight cutoff of 600 Da,[52] thus allowing the passage of small molecules such as the DDC substrate L-Dopa and product dopamine. To investigate the possibility of rapid insertion of OmpF during the prompt formation of polymersomes via film rehydration, we encapsulated horseradish peroxidase (HRP) as a model enzyme that is more stable and easier to work with than DDC. Rehydration solution containing HRP and different concentrations of OmpF (0.02 mg/mL and 0.04 mg/mL) in PBS was used to form HRP-loaded polymersomes with OmpF inserted in the polymeric membrane. As encapsulated HRP catalyses the formation of fluorescent resorufin, a detectable fluorescence signal is only obtained in presence of HRP substrate (Amplex red) when the polymeric membrane is permabilized, demonstrating the proper insertion of OmpF (Figure S4A).[53] Production of resorufin was recorded directly after the addition of Amplex red to a solution of HRP-loaded polymersomes formed in presence of OmpF, while no fluorescence was observed when polymersomes were formed without OmpF (Figure S4B). This demonstrates the functional insertion of OmpF during the rapid formation of polymersomes via film rehydration (Figure S4C), and highlights the ease with which membrane proteins can be inserted into $PDMS_{22}$-$PMOXA_8$-OEG_3-N_3, presumably due the

thinness of the membrane.[48] The extremely rapid polymersome formation (less than 1 min) and simultaneous permeabilization by OmpF insertion during the self-assembly process support our approach to speed polymersomes production in order to minimize the loss of sensitive enzyme (DDC in this case) from the catalytic compartment.

Following these preliminary optimizations using PBS and model enzyme HRP, we proceeded with the encapsulation of our biologically relevant enzyme DDC and optimized the conditions of self-assembly (composition of the rehydration solution, temperature and time). To prevent the degradation of DDC in solution during film rehydration, we added bovine serum albumin (BSA), a commonly used protein stabilizer.[54] We also reconstituted DDC holoenzyme by adding its cofactor pyridoxal phosphate in the rehydration solution. The association of DDC apoenzyme with its cofactor generates the holoenzyme, which is less solvent-accessible, and thus more stable and more compact.[55] As a result, the rehydration solution used to form DDC-Ncomp contained DDC holoenzyme, remaining unbound cofactor pyridoxal phosphate, BSA and OmpF. The obtained DDC-Ncomp formed by rapid film rehydration at room temperature was a mixture of vesicles and worms (Figure S51), probably due to the presence of a large number of molecules in the solution, slowing down self-assembly.[56] A rehydration time of 2 h was necessary to obtain only vesicular-shaped DDC-Ncomp at room temperature (Figure S5B).

To avoid the exposure of DDC to room temperature for 2 h, which can decrease its activity, we investigated the possibility of forming DDC-Ncomp at low temperature (4 °C). After 2 h of rehydration at 4 °C, we obtained a mixture of polymersomes and worms (Figure S5C), presumably due to the slower kinetics of self-assembly at this temperature.[56] An extended rehydration time of 3 h was necessary to obtain only vesicular–shaped DDC-Ncomp (Figure S5D). When DDC-Ncomp was formed under these conditions, the presence of DDC

and BSA in the lumen did not influence the polymersome structure, as judged from TEM micrographs, or the size of DDC-Ncomp, since D_H remained constant (184 ± 66 nm) as determined by DLS (Figure S5D). Systematic investigation of factors affecting the self-assembly process and the enzyme activity (molecular properties of the copolymers and polymersome membrane, self-assembly conditions, stabilizer protein, reconstitution of holoenzyme) led to an optimized procedure to prepare catalytic compartments containing sensitive enzymes, such as DDC-Ncomp (**Figure 2**A).

2.1.3. ssDNA functionalization of polymersomes and clustering of both types of nanocompartments for theranostics

With both imaging and therapeutic nanocompartments in hand, the next step consisted of functionalization with ssDNA to assemble them into theranostic clusters. Here again, different strategies had to be adopted to preserve DDC activity during the ssDNA functionalization of DDC-Ncomp and subsequent formation of clusters. The usage of $PDMS_{22}$-$PMOXA_8$-OEG_3-N_3 copolymer, consisting of short polymer chains less entangled inside the polymersome membrane, promoted the coupling of the ssDNA by increasing the exposure of the azide terminal groups. We used 100 % of this azide-functionalized polymer to obtain the highest density of azide at the surface of polymersomes, thus enabling the attachment of a maximal number of ssDNAs. In addition, we investigated the influence of an additional spacer on the ssDNA sequence in facilitating the formation of dsDNA by hybridization, and thus the clustering of the complementary ssDNA-functionalized polymersomes.

Dye-Ncomp is inherently stable, so its functionalization with ssDNAb or spacer-ssDNAb was accomplished under normal conditions (37 °C, overnight) to obtain maximal

reaction efficiency. To quantify the number of ssDNAb attached per polymersome, ssDNAb labelled with a fluorescent dye (Atto-488) were used to enable detection using fluorescence correlation microscopy (FCS). We confirmed that fluorescently labelled ssDNAb (without DBCO) did not interact with polymersomes, so that the count per molecule obtained for ssDNAb-functionalized Dye-Ncomp reflected only covalently attached ssDNA (Figure S6A) and did not affect the structure of polymersomes (Figure S6B). The number of ssDNAb attached per Dye-Ncomp can be determined by dividing the counts per molecule of ssDNAb-functionalized polymersomes by the counts per molecule of free ssDNAb (Figure S6C). We obtained an average value of 163 ± 61 of ssDNAb per Dye-Ncomp (Figure 2C). Similarly, we determined the density of spacer-ssDNAb as 196 ± 96 spacer-ssDNAb per Dye-Ncomp (Figure 2C, Figure S7).

In order to avoid loss of the catalytic activity of DDC while performing ssDNA functionalization of DDC-Ncomp, we again had to optimize the reaction conditions. As described for DDC-Ncomp formation, we first investigated the feasibility of conducting ssDNA conjugation at 4 °C by using empty polymersomes (rehydrated with PBS only). DY-633-labelled ssDNAa and spacer-DNAa were used to assess the number of ssDNA covalently attached to polymersomes at 4°C during overnight reaction (Figure S7A). The attachment of ssDNAa and spacer-ssDNAa to empty polymersomes was achievable under these conditions (Figure S7B), but the efficiency of the reaction was drastically reduced compared to the conjugation reactions at 37 °C. Under these conditions (4 °C, overnight) for functionalization of DDC-Ncomp, we obtained an average number of 23 ± 6 for ssDNAa and 22 ± 6 for spacer-ssDNAa attached per polymersome (Figure 2C). Note that ssDNA functionalization of the nanocompartments did not affect the architecture of the vesicles or their size, as determined by TEM and DLS (Figure 2D, Figure 2E, Figure S8). Furthermore, the small amount of ssDNAa

present at the surface of DDC-Ncomp should be counterbalanced by the large amount of complementary ssDNAb attached to the Dye-Ncomp, allowing the effective formation of theranostic clusters.

We investigated the cluster formation between DDC-Ncomp and Dye-Ncomp under mild conditions at 20 °C. We compared the clusters formed using polymersomes functionalized with ssDNA and those formed using spacer-ssDNA. After overnight incubation at 20 °C, no clusters were observed in the case of ssDNA-functionalized polymersomes (Figure 2G). In contrast, theranostic clusters formed rapidly when spacer-ssDNA was used. These results support the idea that the spacer enhances the exposure of the complementary ssDNA sequences at the surface of polymersomes, resulting in easier hybridization of complementary strands to trigger the formation of clusters.[37,38] The theranostic clusters formed using spacer-ssDNA rapidly self-organized into sub-micrometer-sized structures that further aggregated after 4 h (Figure 2G). To slow the ssDNA hybridization process, so that the cluster size could be restricted, as well as to minimize loss of DDC activity, we investigated the formation of clusters at 4°C using spacer-ssDNA. But, as no clusters were formed after overnight incubation at 4°C (Figure S9), we decided to control the size of the clusters by shortening the clustering time to 20 min at 20°C; this afforded theranostic clusters of around 500 nm in size (Figure 2H, Figure 2I). These clusters were stored at 4 °C or used immediately. The different strategy adopted to obtain a high density of ssDNAb per Dye-Ncomp enabled us to compensate for the low incorporation of ssDNAa per DDC-Ncomp obtained at the low temperature. Overall, the results indicate that incorporation of a spacer within the ssDNA facilitates the hybridization of ssDNA and promotes the formation of nanotheranostic polymersome clusters.

2.2. Activity and stability of the therapeutic compartment

2.2.1. Kinetic assay for the detection of DDC-triggered production of dopamine

We first estimated the DDC encapsulation efficiency in polymersomes using the model protein BSA, because of its similarity to DDC in size, molecular weight, and solubility (PDB ID: 3V03 and 3RBL); it is also an established model protein for UV-vis absorption measurements[57–59] (see Materials and Methods for further details). We obtained a value of 23.01 ± 6.03 DDC molecules per polymersome, representing an encapsulation efficiency of 15.6 ± 4.12 %, which is consistent with the range of encapsulation efficiencies generally obtained for enzymes within PDMS-PMOXA polymersomes.[53] This provides a concentration of encapsulated DDC of 0.054 µg/mL for DDC-Ncomp and the corresponding clusters.

Having determined the amount of encapsulated DDC per polymersome, we proceeded to assess the production rate of dopamine via irreversible decarboxylation of the substrate L-Dopa under physiological conditions.[60] The production of dopamine by DDC was carried out for up to 24 h in PBS at 37 °C; however, both L-Dopa and dopamine spontaneously auto-oxidize *in vivo*,[61] and this also occurs in PBS, affording a dark, insoluble polydopamine precipitate.[62] To overcome this problem, we decided to add a reducing agent during the DDC-triggered conversion reaction of L-Dopa to dopamine in PBS. We chose glutathione, the most abundant free thiol in mammalian cells, and a major antioxidant in the brain, where it is implicated in the prevention of L-Dopa and dopamine oxidation.[63,64] As expected, no dark precipitate was formed in the presence of glutathione (Figure S10). The assessment of dopamine production by DDC was then possible by HPLC (Figure S11), allowing us to calculate the percent conversion of L-Dopa to dopamine based on the areas under the corresponding peaks (**Figure 3**A). It should be noted that the percentages of conversion recorded all correspond to dopamine production in the µM-mM range (the initial concentration of L-Dopa substrate was 0.49 mM).

2.2.2. Activity of the therapeutic nanocompartment in situ

Free (non encapsulated) DDC was first assessed to verify the role of BSA as a stabilizer. We compared solutions of free DDC containing only DDC diluted in PBS and containing DDC in the presence of 0.1 wt% BSA, corresponding to the BSA concentration used in the rehydration solution to form DDC-Ncomp (Figure 3B, grey and black bars respectively). At all measured time points, the percent conversion of L-Dopa to dopamine in the presence of BSA was higher than in the case of the free DDC alone, confirming that BSA stabilizes DDC.

Considering that the amount of Dopamine produced is closely related to the enzyme concentrations (Figure S12), to compare the activity of free DCC with that of encapsulated DDC inside DDC-Ncomp, as well as DDC-Ncomp clusters, we ensured that DDC was contained at the same concentration (0.05 µg/mL) in all samples. As shown in Figure 3, control DDC-Ncomp without OmpF did not show any conversion of L-Dopa since the polymersome membrane is impermeable (Figure 3B, purple bars). Production of dopamine was observed when DDC was encapsulated in OmpF-equipped DDC-Ncomp, ssDNA functionalized DDC-Ncomp and DDC-Ncomp clusters with the imaging compartment (forming the nanotheranostic system). These results confirm the encapsulation of active DDC inside polymersomes, and the ability of the system to transport and convert L-Dopa and to release therapeutic dopamine (Figure 3B, orange blue and green bars). The percent conversion of L-Dopa to dopamine by encapsulated DDC is lower than that of free DDC in presence of BSA, presumably due to slow diffusion through the channel porin, resulting in a slower reaction *in situ*. The attachment of ssDNAa and subsequent clustering of DDC-Ncomp together with Dye-Ncomp also decreases the efficacy of conversion of L-Dopa to dopamine (Figure 3B, blue and green bars). This decrease in the DDC activity was expected, due to the inherent steric hindrance of OmpF by

the ssDNA and ssDNAa-ssDNAb bridges formed during the polymersome clustering process. Although the DDC-Ncomp-based reporter gene assay is orders of magnitude more sensitive than an HPLC-based system, it is clear that the amount of dopamine (µM) produced by the DNA-linked theragnostic polymersome clusters is within the range required to induce a cellular response (Figure S13). With regards to the reaction kinetics at physiological temperature (37 °C), we compared the conversion of L-Dopa to dopamine by free and encapsulated DDC at the beginning of the reaction (up to 2 h) and after 24 h (Figure 3B). Considering that the L-Dopa substrate is present in excess, the slower conversion rate observed after 24 h is not attributable to a decrease in substrate availability, but should reflect deactivation of the enzyme.

2.2.3. Stability of the therapeutic nanocompartment to thermal deactivation

To gain insight into the thermal stability of DDC, we stored free and encapsulated DDC enzyme at 37 °C for different periods of time (0 to 2 h) prior to the addition of L-Dopa, and then measured dopamine production after 24 h (Figure 3C). Almost no dopamine was produced when free or encapsulated DDC was stored at 37 °C for 2 hours before addition to L-Dopa. These results confirm the rapid thermal inactivation of DDC at 37 °C, and support our explanation of the slower rate of dopamine formation after a longer reaction time at 37°C. To evaluate the stability of free and encapsulated DDC upon storage at a lower temperature, we repeated the same experiment at 4 °C (Figure 3D). The encapsulated DDC maintained a reasonably consistent percent conversion of dopamine up to one week, while free DDC showed a more pronounced decrease in dopamine formation (9.1% loss of dopamine production for free DDC with BSA, compared to 3.5% loss for DDC-Ncomp after 7 days). This behavior can be attributed to the stabilizing effect of polymersomes on DDC, in accordance with previous

findings.[65] Since no activity of encapsulated DDC was retained at 37 °C, we hypothesized that DDC is so sensitive to thermal denaturation that the stabilizing effect of polymersomes is only observable at low temperatures. Thus, even though polymersomes do not extend the active period of encapsulated DDC in PBS at 37°C, they still enhance the stability at 4°C, which may permit longer-term storage – a desirable feature for translational applications.

2.3. Cell response induced by the therapeutic compartment and theragnostic clusters

To investigate the ability of our therapeutic compartment and the theragnostic system of DNA-linked polymersome clusters to produce dopamine *in vitro*, we monitored the response of dopamine-sensing cells during incubation in the presence of DDC-Ncomp and corresponding DNA-linked polymersome clusters. We selected the HEK_{REWARD} double-transgenic cell line as a dopamine-sensing platform; it was previously used to investigate the reward-based control of hypertension via a synthetic brain-dopamine interface.[47] These cells were engineered to ectopically express human dopamine receptor 1 (DRD1), enabling dopamine-triggered production of the reporter, SEAP. SEAP is induced whenever the cells are exposed to dopamine; other metabolically related small molecules, such as L-Dopa, did not trigger DRD1-driven SEAP expression. This HEK_{REWARD} cell line is sensitive to dopamine in the nanomolar range, positioning it as a very sensitive and selective dopamine sensor. It has also been reported that the cellular expression of SEAP was the highest when the cells were incubated with dopamine for 3 days.[47] The delay presumably reflects the fact that the response to dopamine requires time for the cells to initiate the pathways required for SEAP expression. Therefore we chose an incubation time of 3 days for incubation of the DDC-Ncomp and theragnostic polymersome clusters with cells. It should be noted that even though DDC showed reduced

activity after 2 hours at physiological temperature in PBS, the production of dopamine reaches a concentration 31 µM, which is high enough to induce a relevant cell response.

We first investigated the response of HEK_{REWARD} cells when incubated with dopamine alone at various concentrations for 3 days. We observed a linear dependence of cellular expression of SEAP upon dopamine concentration up to 1 µM (Figure S13). No further increase in SEAP expression was observed at higher concentrations of dopamine, and 12 U/L of SEAP was the highest cellular response achieved in our experiments (Figure S13). Second, we investigated the cellular response to dopamine produced by free DDC (**Figure 4**A). The maximum level of SEAP produced was 3 U/L (Figure 4B), probably due to the rapid deactivation of DDC as a result of the cumulative effects of physiological temperature and the cellular milieu. In these cellular assays, no change in SEAP production was observed with free DDC in presence of BSA (Figure 4B) or in PBS buffer only (Figure S14). This lack of a stabilizing effect of BSA on DDC in cell assays could be explained by enhanced sensitivity of DDC under cellular conditions, as well as a dilution effect of BSA with other proteins.

Interestingly, we observed higher levels of SEAP production in the presence of DDC-Ncomp in comparison with free DDC (Figure 4C). Our results clearly indicate the protective role of polymersomes in shielding DDC from attack in the cellular environment (Figure 4C). Within the nanocompartments, BSA can continue to stabilize DDC. DDC-Ncomp functionalized with ssDNAa, and also when present as therapeutic nanocompartments in the DNA-linked theragnostic clusters, successfully induced a cellular response, of the same order of magnitude as DDC-Ncomp (Figure 4D, Figure S15). Notably, in the cell-based assay, the presence of ssDNAa and the location of DDC-Ncomp in theragnostic clusters appears to compensate for the reduced activity observed in PBS, in agreement with other studies showing that catalytic nanocompartments were more active in cell media than in PBS as compared to

free enzymes.[53] This effect is most likely due to the shielding of polymersomes and to the presence of ssDNAa on the surface of the polymersomes, promoting the attachment of single polymersomes and DNA-zipped polymersome clusters to the cell membrane.[62] This point will be discussed in more detail in the following section. Such proximity with the cell membrane eventually leads to a locally increased concentration of dopamine near the DRD1 receptors, resulting in an increase of SEAP expression.

2.4. Tracking the behavior of polymersome clusters in the presence of cells via the imaging compartment

We previously showed that DNA-zipped clusters possess interesting surface-binding ability to epithelial cells due to their physical properties.[38] Their softness, increased size (unfavourable for endocytosis), and availability of ssDNA on the surface promote their attachment to scavenger receptors present at the surface of epithelial cells. Scavenger receptors are known to bind DNA, RNA and other negatively charged large molecules.[66] Zeta potential measurements of our nanocompartments confirmed that ssDNA-functionalized polymersomes were more negatively charged (- 13.53 ± 2.54 mV for Dye-Ncomp and - 6. 93 ± 3.38 mV for DDC-Ncomp) than non ssDNA-functionalized polymersomes (- 5.24 ± 0.4 mV), thus making them prime candidates for attachment to scavenger receptors. Since the HEK_{REWARD} cell line used for our experiments is of epithelial origin, it should interact with ssDNA-functionalized polymersomes and clusters. To investigate the interaction between the DNA-linked polymersome clusters and this new engineered HEK_{REWARD} cell line, we used ssDNA-functionalized polymersomes or DNA-linked polymersome clusters loaded with fluorescent dyes (DY-633 and Atto-488) as imaging compartments. The binding efficiency of spacer-ssDNA-bearing single polymersomes and DNA-linked polymersome clusters was investigated using CLSM, at the same

concentrations as used for the cellular assay. As expected, the single imaging compartments functionalized with spacer-ssDNA bound to the cell surface of HEK_{REWARD}, whereas non-functionalized polymersomes showed lower attachment (Figure S16). To investigate whether the clusters also bind to the cell surface, as was the case for the functionalized polymersomes, we loaded the therapeutic compartment with Atto-488 for visualization purposes and kept the imaging compartment loaded with DY-633 as described above (**Figure 5**). We incubated these dye-loaded clusters in the presence of the cells for 24 hours, then washed and imaged the cells to assess not only binding to the cell surface, but also whether or not the clusters maintain their bound conformation. For the theranostic system to function, it is imperative that the clustered architecture is maintained and that the two compartments coexist, functioning in unison. After incubation with the cells and rigorous washing, we could indeed observe the colocalization of the Atto-488 and DY-633 compartments, with a Pearson's colocalization coefficient of 0.77 ± 0.09. The co-localisation observed for the two different compartments of the clusters demonstrates clustering of the nanocompartments and the stability of the DNA linkers *in vitro* (Figure S17*)*. Considering the sensitivity and low lifetime of DDC, we wanted to determine how fast cell binding of the clusters occurs, as this would determine the overall efficacy of our system. For this experiment, we incubated the cells in the presence of the dye-loaded clusters and observed their attachment via CLSM live imaging. The results indicate that the cell binding process is fast, as fluorescence was apparent at the cell membrane within 10 min, and continued to increase thereafter (Figure S18). The fast binding of the DNA-linked polymersome clusters to the cell surface, before thermal deactivation of DDC can occur, is what leads to the locally enhanced production of dopamine, thus resulting in higher SEAP production as compared to that of the free enzyme observed in the cellular assay. This observation also confirms the ability

of the dye-Ncomp to track itself and polymersome clusters over time in a biologically relevant milieu, supporting its robustness and potency as an imaging compartment.

3. Conclusion

Here we engineered a novel platform composed of segregated catalytic and imaging polymeric compartments linked together via DNA hybridization to form a modular nanotheranostic system. A combination of optimized construction strategies, i.e., 1) high polymer concentration, 2) short block-copolymers, 3) short rehydration time, and 4) low temperature, coupled with mild encapsulation conditions, permits the effective loading of DDC in the lumen of polymersomes, affording the active therapeutic compartment (DDC-Ncomp) that is able to produce dopamine in PBS and cell media. The surface functionalization of DDC-Ncomp with DNA was also successfully achieved under mild conditions where DDC was not substantially degraded, even though the amount of DNA attached was relatively low. The polymersomes protect DDC activity sufficiently during storage at 4 °C and also in cell media. As a result, active polymersomes encapsulating DCC and corresponding clusters are able to trigger a cellular response via dopamine production and activation of dopamine receptors, and the response is considerably enhanced compared to the case of free DDC. By employing a modular system, we were able to assemble the imaging compartment (Dye-Ncomp) under harsher conditions that permitted a high encapsulation efficiency of the stable DY-633 dye and an increase in amount of attached DNA on the polymersome surface, compared to DDC-Ncomp. This enabled the successful formation of theranostic clusters via DNA-zipping. The presence of DNA on the surface of DDC-Ncomp affects the dopamine production rate by hindering the passage of substrate through the OmpF pore, but interestingly, in cell experiments, this DNA-associated loss of activity is compensated in the case of the theranostic clusters by the focused

production of dopamine in close proximity to the dopamine D1 receptor. DNA promotes the attachment of polymersomes and clusters at the surface of epithelial cells, leading to an increased local concentration of dopamine at the cell surface, followed by efficient receptor activation. From a therapeutic point of view, dopamine activation of cell-surface dopamine D1 receptor molecules present on peripheral arteries has been shown to prevent atherosclerosis.[41–43] Secondly, atherosclerosis can be regarded as a chronic inflammatory state that involves the presence of scavenger receptor-expressing macrophages in locations where atherosclerotic lesions are formed.[45,67] By attaching the nanotheranostic clusters to these macrophages, we may be able to detect the early stages of artherosclerotic plaque formation as well as generate dopamine, preventing progression of the disease. Most current treatments and detection methods for atherosclerosis are invasive and inadequate[68] and therefore an early detection and prevention system such as our nanotheranostic platform could provide a much-needed alternative. Further, since our system is modular, it should be possible to extend its applicability to other disease states.

4. Experimental Section

Materials: DBCO-ss-DNA sequences were purchased from IBA Lifesciences (Göttingen, Germany). DDC was purchased from Biotechne (Zug, Switwerland). Dulbecco's PBS was purchased from BioConcept (Allschwill, Switzerland). L-Dopa (levodopa), dopamine hydrochloride, pyridoxal 5'-phosphate monohydrate, BSA, reduced L-glutathione, diethanolamine, L-homoarginine, magnesium chloride, and *p*-nitrophenyl phosphate were obtained from Sigma-Aldrich (St. Louis, USA). N-Octyl-β-D-glucoside was purchased from Anatrace (Maumee, USA). The fluorescent probes Atto-488 and DY-633 were purchased from

ATTO-TEC GmbH (Siegen, Germany) and Dyomics GmbH (Jena, Germany), respectively. All compounds and solvents were used as received.

Synthesis of $PDMS_{22}$-$PMOXA_8$-OEG_3-N_3: $PDMS_{22}$-$PMOXA_8$ with a hydroxyl functional group ($PDMS_{22}$-$PMOXA_8$-OH) was synthesized accordingly to the well-established protocol of our research group.[69] $PDMS_{22}$-$PMOXA_8$ with azide as the end functional group ($PDMS_{22}$-$PMOXA_8$-N_3) was synthesized accordingly our recently published procedure[37] with slight modifications. Briefly, $PDMS_{22}$-$PMOXA_8$-OH (350 mg) was first dissolved in 10 mL anhydrous chloroform at RT, then succinic anhydride (30 mg,), 4-dimethylaminopyridine (5 mg) and TEA (30 µL) were added successively. The mixture was deoxygenated by means of three vacuum-argon cycles, and then stirred for another 72 h at room temperature under Ar. Ultrafiltration afforded colorless $PDMS_{22}$-$PMOXA_8$ with a carboxylic acid end group ($PDMS_{22}$-$PMOXA_8$-COOH) (yield: 300 mg, 86%). This $PDMS_{22}$-$PMOXA_8$-COOH (300 mg) was dissolved in anhydrous chloroform at room temperature, then 11-azido-3,6,9-trioxaundecan-1-amine (50 mg), N,N'-dicyclohexylcarbodiimide (46 mg) and 4-dimethylaminopyridine (3 mg) were added to the solution. The mixture was deoxygenated three times, then stirred at 30 rpm for another 48 h at RT. Ultrafiltration afforded colorless $PDMS_{22}$-$PMOXA_8$-N_3 (yield: 220 mg, 73%).

Rapid formation of $PDMS_{22}$-$PMOXA_8$-OEG_3-N_3 polymersomes: $PDMS_{22}$-$PMOXA_8$-OEG_3-N_3 block copolymers were dissolved in ethanol to yield a stock solution with a concentration of 10 mg/mL. 400 µL of this solution was transferred into a 5 mL round-bottomed flask, and dried in a rotary evaporator (170 mbar, 40 ˚C, 75 rpm). 1 mL of PBS was added to the residue, and the flask was gently shaken with stirring bar for less than 1 min at RT. The resulting solution was

extruded 15 times through a polycarbonate (PC) membrane with a 200 nm diameter pore size on an Avanti mini-extruder (Avanti Polar Lipids, Alabama, USA) to unify the size of the polymersomes.

Conjugation of DNA with empty polymersomes: Empty polymersomes (4 mg/mL) were mixed with 1 eq. per azide group of ssDNAa or spacer-ssDNAa labelled with DY-633 (0.5 mM in water). The reaction was carried out overnight at 4 °C. Free DNA was removed by size exclusion chromatography (SEC) eluted with PBS.

Preparation of HRP-Ncomp: $PDMS_{22}$-$PMOXA_8$-OEG_3-N_3 stock solution (200 µL, 10 mg/mL) was transferred into a 5 mL round-bottomed flask, and dried on a rotary evaporator (170 mbar, 40 ˚C, 75 rpm). HRP solution (100 µL, 0.2 mg/mL) containing 0.1 wt% BSA with either PBS (100 µL) or OmpF (100 µL, 0.1 mg/mL or 0.2 mg/mL) was added to the residue, resulting in a final concentration of 0.16 mg/mL of HRP, 4 mg/mL of $PDMS_{22}$-$PMOXA_8$-OEG_3-N_3 and 0 mg/mL, 0.02 mg/mL, and 0.04 mg/mL of OmpF. The flask was gently shaken with a stirring bar for less than 10 seconds at room temperature. The resultant HRP-Ncomp was extruded the same way as described for the empty polymersomes. Free HRP was removed by means of SEC, eluted with PBS.

Activity of HRP-Ncomp: HRP-Ncomp (10 µg/mL) was incubated in the presence of H_2O_2 (10 µM) in a 96-well black plate (Thermo Fisher Scientific), before the addition of Amplex Red (1 µM) to give a final volume of 200 µL/well. The change of fluorescence (excitation 570 nm / emission 595 nm) after the addition of Amplex Red was recorded immediately using a Spectramax M5 microplate reader (Molecular Devices, USA).

Preparation of DDC-Ncomp: A solution of $PDMS_{22}$-$PMOXA_8$-OEG_3-N_3 polymer dissolved in ethanol (600 µL, 10 mg/mL) was transferred into a 5 mL round-bottomed flask, and dried on a rotary evaporator (170 mbar, 40 ˚C, 75 rpm). In parallel, freshly thawed DDC (20 µg) was dissolved in 0.1 wt% BSA in PBS (1 mL) and pyridoxal phosphate in PBS (50 µL, 5 mM). The mixture was gently stirred at 4°C for 20 min. The thin polymer film was rehydrated with this DDC solution (522 µL) mixed with dialyzed OmpF solution (78 µL, 0.8 mg/mL to give the same polymer/OmpF ratio as used for HRP-Ncomp) (see the SI for further details). The resulting solution was stirred 3 hours at 4 °C, and then extruded 15 times through a PC membrane with a 200 nm diameter pore size under sterile conditions to unify the size of the polymersomes.

DDC encapsulation efficiency: Polymersomes encapsulating BSA (BSA-Ncomp) were formed under the same conditions described above, but using BSA in place of DDC and using PBS only (without further 0.1wt% BSA). The concentration of non-encapsulated BSA was determined from the fraction of free BSA present in the solution after SEC purification of BSA-Ncomp. Polymersomes rehydrated under the same conditions but without BSA were also formed and purified for use as a blank. After UV-vis (280 nm) absorbance measurements using a NanoDrop 2000 spectrophotometer (Thermofisher) in BSA mode, we determined the amount of BSA molecules encapsulated in polymersomes. We calculated the difference between the total amount of BSA used for film rehydration and the amount of non-encapsulated BSA, which gave a number of $1.79*10^{13} \pm 4.71*10^{12}$ molecules of BSA encapsulated. In parallel, the concentration of vesicles ($1.3*10^{12}$ vesicles/mL) was determined via single nanoparticle tracking analysis (NTA) using a NanoSight NS300 instrument from Malvern Panalytical

(Malvern, United Kingdom). We divided the number of encapsulated BSA molecules by the number of vesicles in our solution (600 µL), obtaining a value of 23.01 ± 6.03 BSA molecules encapsulated per vesicle. Assuming similar numbers of BSA and DDC, the percentage of DDC encapsulation is calculated to be 15.6 ± 4.12 %.

OmpF expression and extraction: Wild-type OmpF was obtained according to a previously reported protocol,[53] with a few modifications: bacteria were grown at 30 °C for 6 h on Terrific Broth (TB) (Difco, U.S.A.), and all ultracentrifugations were performed at room temperature.

Preparation of Dye-Ncomp: A stock solution of $PDMS_{22}$-$PMOXA_8$-OEG_3-N_3 block copolymer was obtained by dissolution of the polymer in ethanol (600 µL, 10 mg/mL), and transferred to a round-bottomed flask, followed by drying on a rotary evaporator (170 mbar, 40 ˚C, 75 rpm). The resultant thin polymer film was rehydrated by adding a solution of DY-633 (600 µL, 0.2 mM in PBS). The product was stirred overnight at room temperature before being extruded in the same way as described for DDC-Ncomp.

DNA conjugation and cluster formation: Extruded DDC-Ncomp and Dye-Ncomp (500 µL each) were mixed with 1 eq. per azide group of ssDNA/spacer-ssDNAa (0.5 mM in water) overnight (4 °C) and ssDNAb/spacer-ssDNAb (0.5 mM in water) overnight (37 °C), respectively. The two solutions were purified by means of SEC to remove free DNA, under sterile conditions, and cold PBS. The volumes of purified polymersomes solutions were adjusted to obtain a polymer concentration of 2 mg/mL. To prepare clusters, the two solutions were mixed (1:1) and incubated at 20 °C for 20 min. The resulting cluster solution was used immediately.

Transmission electron microscopy (TEM): A 5 μL aliquot of polymersomes or polymersome clusters (0.1 mg/mL) was absorbed on 400 mesh square copper grids. The grids were further stained with 2% uranyl acetate and the negatively stained image of nanostructures was obtained with a transmission electron microscope (Philips CM100) at an accelerating voltage of 80 kV.

Dynamic light scattering (DLS): The apparent D_H values of polymersomes and polymersome clusters were obtained on a Zetasizer Nano ZSP (Malvern Instruments Inc., UK) at 25 °C. 400 μL of each sample solution (0.2 mg/mL final concentration) was added to a cuvette and subjected to 11 runs repeated three times. The measured angle was 173° and the data was analyzed by number distribution. To examine the kinetics of polymersome cluster formation, measurements were run for 3 min with a 2 min interval.

Zeta potential measurement: The electrophoretic mobility of vesicles in solution was determined by means of laser Doppler velocimetry and phase-analysis light-scattering measurements. A Malvern Zetasizer Nano ZSP (Malvern Instruments Inc, UK) with a 633 nm wavelength laser was used for all measurements. The vesicle samples (0.2 mg/mL) were measured in PBS with five repeat measurements per sample. All experiments were run at 25 °C.
Static light scattering (SLS): Multi-angle dynamic light scattering (DLS) and static light scattering (SLS) were performed on a setup from LS Instruments (Switzerland), equipped with a 21 mW He-Ne laser (λ = 632.8 nm) for scattering angles from 30° to 150° at 25 °C. All samples were diluted in order to suppress multiple scattering. Second-order cumulant analysis for various angles was performed to obtain the hydrodynamic radius (Rh). The radius of gyration (Rg) was obtained from the SLS data using a Guinier plot.

Fluorescence Correlation Spectroscopy (FCS): FCS was performed on a Zeiss LSM 880 microscope (Zeiss LSM 880, inverted microscope ZEISS Axio Observer, Carl Zeiss, Jena, Germany). A 488 nm argon laser was used to excite ssDNA labelled with Atto-488 and the conjugated Ncomp. The laser beam was passed through main beam splitter MBS488 and signals were detected in the range of 500-532 nm. A 633 nm HeNe laser, was used for DY-633 labelled ssDNA and the conjugated Ncomp. The laser beam was passed through MBS488/561/633 filter and the signal was detected in the range of 650-740 nm, the pinholes were adjusted to maximize the count rate using the corresponding free dye in PBS. The sample volume was 15 µL. Fluorescence fluctuations over time were recorded for 30 x 10 s. The raw data was processed and analyzed using Zeiss software. Autocorrelation curves were fitted to a two-component model (Equation S1).

$$G_{2comp}(\tau) = 1 + \frac{1}{N} \cdot \left(1 + \frac{T_{trip}}{1-T_{trip}} \mathrm{e}^{-\frac{\tau}{\tau_{trip}}}\right) \cdot \left[\frac{\mathrm{f}_1}{\left(1+\frac{\tau}{\tau_{D_1}}\right)\left(1+\frac{\tau}{S^2\tau_{D_1}}\right)^{1/2}} + \frac{\mathrm{f}_2}{\left(1+\frac{\tau}{\tau_{D_2}}\right)\left(1+\frac{\tau}{S^2\tau_{D_2}}\right)^{1/2}}\right] \quad (1)$$

Where $G_{2comp}(\tau)$ is the two-component autocorrelation function, *N* is the number of particles, S is the structural parameter, T_{trip} is the fraction of fluorophores in the triplet state, τ_{trip} is the corresponding triplet time, f_1 and f_2 are the fractions of the particles of the corresponding component 1 or 2, and τ_{D_1} and τ_{D_2} are the diffusion times of the corresponding component 1 or 2.

Confocal laser scanning microscopy (CLSM): CLSM measurements were recorded on a confocal laser-scanning microscope (ZEISS LSM 880, inverted microscope ZEISS Axio Observer, Carl Zeiss, Germany). For visualizing polymersome clusters in the presence of cells, the two Ncomps were loaded with Atto-488 and DY-633, respectively, and two lasers, a 488

nm argon laser and a 633 nm HeNe laser, were used. The beams were passed through MBS488 and MBS488/561/633 filters, respectively, and focused onto the sample through a water immersion objective (C-Apochromate 40x/1.2W korr FCS M27). Detection was done at 505-555 nm and 650-740 nm, respectively. For polymersome clusters formed from DDC-Ncomp and dye-Ncomp, only the 633 nm HeNe laser was utilized.

Activity determination of the therapeutic compartment: 80 µL of purified 1 mg/mL of DDC-Ncomp, DDC-Ncomp functionalized with ssDNA, theragnostic clusters or DDC-Ncomp without OmpF was mixed with 10 µL of L-dopa (5 mM in water), 10 µL of reduced glutathione (20 mM in PBS) and 2 µL of pyridoxal phosphate (5 mM in water), and incubated 24 h at 37 °C. Then, each solution was purified by SEC to remove the polymersomes, and analysed by reverse-phase HPLC to detect the presence of dopamine. The percentage conversion of L-Dopa to dopamine was calculated from the areas of the corresponding peaks: for every sample, the area of the dopamine peak is multiplied by 100 and divided by the sum of the areas of the dopamine and L-Dopa peaks. This approach was chosen to avoid potential errors in the assessment of L-Dopa and dopamine concentrations due to sample dilution during SEC purification, which was required to prevent injection of vesicles into the HPLC.

HPLC: The retention times for dopamine and L-Dopa were determined using a reverse-phase Shimadzu HPLC (Reinach, Switzerland). A 20-min method using water containing 0.1% TFA as a mobile phase at 0.5 mL/min though an analytical Chromolith performance RP-18e column (Merck, Schaffhausen, Switzerland) separated dopamine (10.1 min) and L-Dopa (11.8 min) (Figure S7). At equal concentrations, the peaks corresponding to dopamine and L-Dopa showed similar areas. Detection was done at 280 nm.

Cell culture: The stable double-transgenic cell line HEK_{REWARD} was cultured in Dulbecco's modified Eagle's medium GlutaMAX^{TM}-I (DMEM-GlutaMAX, Gibco Life Sciences) supplemented with 10% FCS (BioConcept), 100 units/mL penicillin and 100 µg/mL streptomycin (Sigma Aldrich). After 14 days, the polyclonal population was selected according to reported methodology.[47] Cells were maintained at 37 °C in a humidified atmosphere of 5% CO_2 in air.

Cellular attachment and imaging: Freshly trypsinized cells were seeded at a density of 60 000 cells per well, in 8-well ibidi collagen IV-coated plates. After 24 h, the cell culture medium was removed and replaced with 130 µL Opti-MEM (Gibco Life Sciences) live cell imaging medium. Next, cells were dosed with polymersome clusters (70 µL, 2 mg/mL) and imaged by CLSM at intervals for 2 h. CLSM measurements were performed on a ZEISS LSM 880 inverted microscope (ZEISS Axio Observer, Carl Zeiss, Germany) with a water immersion objective C-Apochromate 40x/1.2W korr FCS M27. For Atto-488, the beam from a 488 nm argon laser was passed through a main beam splitter MBS488; detection was done at 499-643 nm. For DY-633, the HeNe 633 nm laser beam was passed through MBS488/561/633 filters and detection was done at 638-759 nm.

For the 24 hour time points, freshly trypsinized cells were seeded at a density of 30 000 cells per well in 8-well ibidi collagen IV-coated plates. After 24 h, cells were treated with the polymersome clusters as previously described. After a further 24 h incubation, the cells were washed 3x with Opti-MEM prior to CLSM imaging. Images were processed using Fiji ImageJ and colocalization analysis based on Pearson's coefficient of colocalization was performed using the JACoP plugin.

Cell activation by DDC-Ncomp and theragnotic clusters: Cells were plated in a 96-well plate (100 µL/well of 10 000 cells) and incubated overnight. The next day, 75 µL of media was removed and 75 µL of free DDC (different concentrations) or 1 mg/mL of DDC-Ncomp w/o OmpF, DDC-Ncomp, ssDNA-functionalized DDC-Ncomp or theragnostic clusters was added to the wells. Wells were filled with 100 µL of media containing L-dopa (10 µM) and pyridoxal phosphate (12.5 µM) and incubated for 3 days. Then, the SEAP level was assayed using a standard *p*-nitrophenyl phosphate–based absorbance method as previously described.[70] In brief, the cell supernatant corresponding to each condition was assayed by recording the rate of production of p-nitrophenol from the SEAP substrate *p*-nitrophenyl phosphate, calculated from the absorbance at 405 nm. The amount of SEAP expressed under each condition was calculated using the slope of the kinetic curve of *p*-nitrophenol production.

Supporting Information

Supporting Information is available from the Wiley Online Library or from the author.

Acknowledgements

We gratefully acknowledge financial support from the Swiss National Science Foundation, NCCR-MSE and the University of Basel. The authors thank Andrea Belluati for providing OmpF. Prof. Wolfgang Meier (University of Basel) is acknowledged for helpful and detailed discussions. Author 1 and Author 2 contributed equally to this work.

Received: ((will be filled in by the editorial staff))

Revised: ((will be filled in by the editorial staff))

Published online: ((will be filled in by the editorial staff))

References

[1] E.-K. Lim, T. Kim, S. Paik, S. Haam, Y.-M. Huh, K. Lee, *Chem. Rev.* **2015**, *115*, 327.

[2] H. Chen, W. Zhang, G. Zhu, J. Xie, X. Chen, *Nat. Rev. Mater.* **2017**, *2*, 1.

[3] S. K. Golombek, J.-N. May, B. Theek, L. Appold, N. Drude, F. Kiessling, T. Lammers, *Adv. Drug Deliv. Rev.* **2018**, *130*, 17.

[4] B. T. Luk, L. Zhang, *ACS Appl. Mater. Interfaces* **2014**, *6*, 21859.

[5] P. Zou, Y. Yu, Y. A. Wang, Y. Zhong, A. Welton, C. Galbán, S. Wang, D. Sun, *Mol. Pharm.* **2010**, *7*, 1974.

[6] J. Yang, G. Gao, X. Zhang, Y.-H. Ma, H.-R. Jia, Y.-W. Jiang, Z. Wang, F.-G. Wu, *Nanoscale* **2017**, *9*, 15441.

[7] S. Sahu, N. Sinha, S. K. Bhutia, M. Majhi, S. Mohapatra, *J. Mater. Chem. B* **2014**, *2*, 3799.

[8] Q. He, M. Ma, C. Wei, J. Shi, *Biomaterials* **2012**, *33*, 4392.

[9] S. Santra, C. Kaittanis, J. Grimm, J. M. Perez, *Small* **2009**, *5*, 1862.

[10] T. D. Schladt, M. I. Shukoor, K. Schneider, M. N. Tahir, F. Natalio, I. Ament, J. Becker, F. D. Jochum, S. Weber, O. Köhler, P. Theato, L. M. Schreiber, C. Sönnichsen, H. C. Schröder, W. E. G. Müller, W. Tremel, *Angew. Chem. Int. Ed.* **2010**, *49*, 3976.

[11] A. O. Elzoghby, A. L. Hemasa, M. S. Freag, *J. Controlled Release* **2016**, *243*, 303.

[12] F. Scaletti, J. Hardie, Y.-W. Lee, D. C. Luther, M. Ray, V. M. Rotello, *Chem. Soc. Rev.* **2018**, *47*, 3421.

[13] J. Li, X. Chang, X. Chen, Z. Gu, F. Zhao, Z. Chai, Y. Zhao, *Biotechnol. Adv.* **2014**, *32*, 727.

[14] J. R. Upponi, K. Jerajani, D. K. Nagesha, P. Kulkarni, S. Sridhar, C. Ferris, V. P. Torchilin, *Biomaterials* **2018**, *170*, 26.

[15] K. Bruun, C. Hille, *Sci. Rep.* **2019**, *9*, 1.

[16] C. Yao, P. Wang, X. Li, X. Hu, J. Hou, L. Wang, F. Zhang, *Adv. Mater.* **2016**, *28*, 9341.

[17] L. Sercombe, T. Veerati, F. Moheimani, S. Y. Wu, A. K. Sood, S. Hua, *Front. Pharmacol.* **2015**, *6*, 286.

[18] F. Wang, J. Gao, J. Xiao, J. Du, *Nano Lett.* **2018**, *18*, 5562.

[19] B. M. Geilich, A. L. van de Ven, G. L. Singleton, L. J. Sepúlveda, S. Sridhar, T. J. Webster, *Nanoscale* **2015**, *7*, 3511.

[20] T. Anajafi, S. Mallik, *Ther. Deliv.* **2015**, *6*, 521.

[21] C. G. Palivan, R. Goers, A. Najer, X. Zhang, A. Car, W. Meier, *Chem. Soc. Rev.* **2016**, *45*, 377.

[22] J. Leong, J. Y. Teo, V. K. Aakalu, Y. Y. Yang, H. Kong, *Adv. Healthc. Mater.* **2018**, *7*, 1701276.

[23] M. Mohammadi, M. Ramezani, K. Abnous, M. Alibolandi, *Int. J. Pharm.* **2017**, *519*, 287.

[24] H. Zhang, W. Cui, X. Qu, H. Wu, L. Qu, X. Zhang, E. Mäkilä, J. Salonen, Y. Zhu, Z. Yang, D. Chen, H. A. Santos, M. Hai, D. A. Weitz, *Proc. Natl. Acad. Sci.* **2019**, *116*, 7744.

[25] A. Belluati, I. Craciun, C. E. Meyer, S. Rigo, C. G. Palivan, *Curr. Opin. Biotechnol.* **2019**, *60*, 53.

[26] O. Rifaie-Graham, S. Ulrich, N. F. B. Galensowske, S. Balog, M. Chami, D. Rentsch, J. R. Hemmer, J. Read de Alaniz, L. F. Boesel, N. Bruns, *J. Am. Chem. Soc.* **2018**, *140*, 8027.

[27] H. Che, S. Cao, J. C. M. van Hest, *J. Am. Chem. Soc.* **2018**, *140*, 5356.

[28] K. Langowska, C. G. Palivan, W. Meier, *Chem. Commun.* **2012**, *49*, 128.

[29] P. Tanner, V. Balasubramanian, C. G. Palivan, *Nano Lett.* **2013**, *13*, 2875.

[30] T. Einfalt, D. Witzigmann, C. Edlinger, S. Sieber, R. Goers, A. Najer, M. Spulber, O. Onaca-Fischer, J. Huwyler, C. G. Palivan, *Nat. Commun.* **2018**, *9*, 1.

[31] M. Li, Z. Luo, Y. Zhao, *Chem. Mater.* **2018**, *30*, 25.

[32] M. Sun, L. Xu, W. Ma, X. Wu, H. Kuang, L. Wang, C. Xu, *Adv. Mater.* **2016**, *28*, 898.

[33] X. Yang, J. Xiong, P. Qiu, M. Chen, D. He, X. He, K. Wang, J. Tang, *RSC Adv.* **2017**, *7*, 7742.

[34] R. Tang, C. S. Kim, D. J. Solfiell, S. Rana, R. Mout, E. M. Velázquez-Delgado, A. Chompoosor, Y. Jeong, B. Yan, Z.-J. Zhu, C. Kim, J. A. Hardy, V. M. Rotello, *ACS Nano* **2013**, *7*, 6667.

[35] X. J. Loh, T.-C. Lee, Q. Dou, G. R. Deen, *Biomater. Sci.* **2015**, *4*, 70.

[36] P. Tanner, O. Onaca, V. Balasubramanian, W. Meier, C. G. Palivan, *Chem. – Eur. J.* **2011**, *17*, 4552.

[37] J. Liu, V. Postupalenko, S. Lörcher, D. Wu, M. Chami, W. Meier, C. G. Palivan, *Nano Lett.* **2016**, *16*, 7128.

[38] I. Craciun, J. Liu, A. Belluati, T. Einfalt, S. Sieber, D. Witzigmann, C. G. Palivan, Zurich, **2018**.

[39] S. H. Snyder, *Proc. Natl. Acad. Sci.* **2011**, *108*, 18869.

[40] K. Yasunari, M. Kohno, H. Kano, K. Yokokawa, M. Minami, J. Yoshikawa, *J. Atheroscler. Thromb.* **1997**, *4*, 59.

[41] Yasunari Kenichi, Kohno Masakazu, Hasuma Tadayoshi, Horio Takeshi, Kano Hiroaki, Yokokawa Koji, Minami Mieko, Yoshikawa Junichi, *Arterioscler. Thromb. Vasc. Biol.* **1997**, *17*, 3164.

[42] Y. Zhou, W. Shi, H. Luo, R. Yue, Z. Wang, W. Wang, L. Liu, W. E. Wang, H. Wang, C. Zeng, *Hypertens. Res.* **2015**, *38*, 807.

[43] Y. Yao, D. Yang, Y. Han, W. Wang, N. Wang, J. Yang, C. Zeng, *Cell. Physiol. Biochem.* **2016**, *38*, 415.

[44] J. Frostegård, *BMC Med.* **2013**, *11*, 117.

[45] Y. V. Bobryshev, E. A. Ivanova, D. A. Chistiakov, N. G. Nikiforov, A. N. Orekhov, *Biomed. Res. Int.* **2016**.

[46] K. J. Moore, I. Tabas, *Cell* **2011**, *145*, 341.

[47] K. Rössger, G. C.-E. Hamri, M. Fussenegger, *Proc. Natl. Acad. Sci.* **2013**, *110*, 18150.

[48] F. Itel, A. Najer, C. G. Palivan, W. Meier, *Nano Lett.* **2015**, *15*, 3871.

[49] E. M. Sletten, C. R. Bertozzi, *Acc. Chem. Res.* **2011**, *44*, 666.

[50] K. H. PhD, R. A. H. Surtees, C. R. MD, P. T. Clayton, *Neurology* **1992**, *42*, 1980.

[51] A. Najer, D. Wu, A. Bieri, F. Brand, C. G. Palivan, H.-P. Beck, W. Meier, *ACS Nano* **2014**, *8*, 12560.

[52] G. Kefala, C. Ahn, M. Krupa, L. Esquivies, I. Maslennikov, W. Kwiatkowski, S. Choe, *Protein Sci.* **2010**, *19*, 1117.

[53] A. Belluati, I. Craciun, J. Liu, C. G. Palivan, *Biomacromolecules* **2018**, *19*, 4023.

[54] B. S. Chang, R. R. Mahoney, *Biotechnol. Appl. Biochem.* **1995**, *22*, 203.

[55] G. Giardina, R. Montioli, S. Gianni, B. Cellini, A. Paiardini, C. B. Voltattorni, F. Cutruzzolà, *Proc. Natl. Acad. Sci.* **2011**, *108*, 20514.

[56] Y. Mai, A. Eisenberg, *Chem. Soc. Rev.* **2012**, *41*, 5969.

[57] S. V. Thakkar, K. M. Allegre, S. B. Joshi, D. B. Volkin, C. R. Middaugh, *J. Pharm. Sci.* **2012**, *101*, 3051.

[58] H. Xu, N. Yao, H. Xu, T. Wang, G. Li, Z. Li, *Int. J. Mol. Sci.* **2013**, *14*, 14185.

[59] V. D. Suryawanshi, L. S. Walekar, A. H. Gore, P. V. Anbhule, G. B. Kolekar, *J. Pharm. Anal.* **2016**, *6*, 56.

[60] A. Gjedde, J. Reith, S. Dyve, G. Léger, M. Guttman, M. Diksic, A. Evans, H. Kuwabara, *Proc. Natl. Acad. Sci.* **1991**, *88*, 2721.

[61] M. Asanuma, I. Miyazaki, N. Ogawa, *Neurotox. Res.* **2003**, *5*, 165.

[62] H. Lee, S. M. Dellatore, W. M. Miller, P. B. Messersmith, *Science* **2007**, *318*, 426.

[63] A. Meister, M. E. Anderson, *Annu. Rev. Biochem.* **1983**, *52*, 711.

[64] Z. D. Zhou, T. M. Lim, *Neurochem. Res.* **2009**, *34*, 316.

[65] D. C. L. Chierico, X. Tian, K. Kluthe, A. Poma, L. Ruiz-Pérez, C. LoPresti, G. Battaglia, **2016**, arxiv.org/abs/1607.08886. arXiv e-Print archive

[66] N. Platt, S. Gordon, *Chem. Biol.* **1998**, *5*, R193.

[67] K. J.Moore, M. W. Freeman, *Arterioscler. Thromb. Vasc. Biol.* **2006**, *26*, 1702.

[68] W. Slijkhuis, W. Mali, Y. Appelman, *Neth. Heart J.* **2009**, *17*, 140.

[69] D. Wu, M. Spulber, F. Itel, M. Chami, T. Pfohl, C. G. Palivan, W. Meier, *Macromolecules* **2014**, *47*, 5060.

[70] S. Schlatter, M. Rimann, J. Kelm, M. Fussenegger, *Gene* **2002**, *282*, 19.

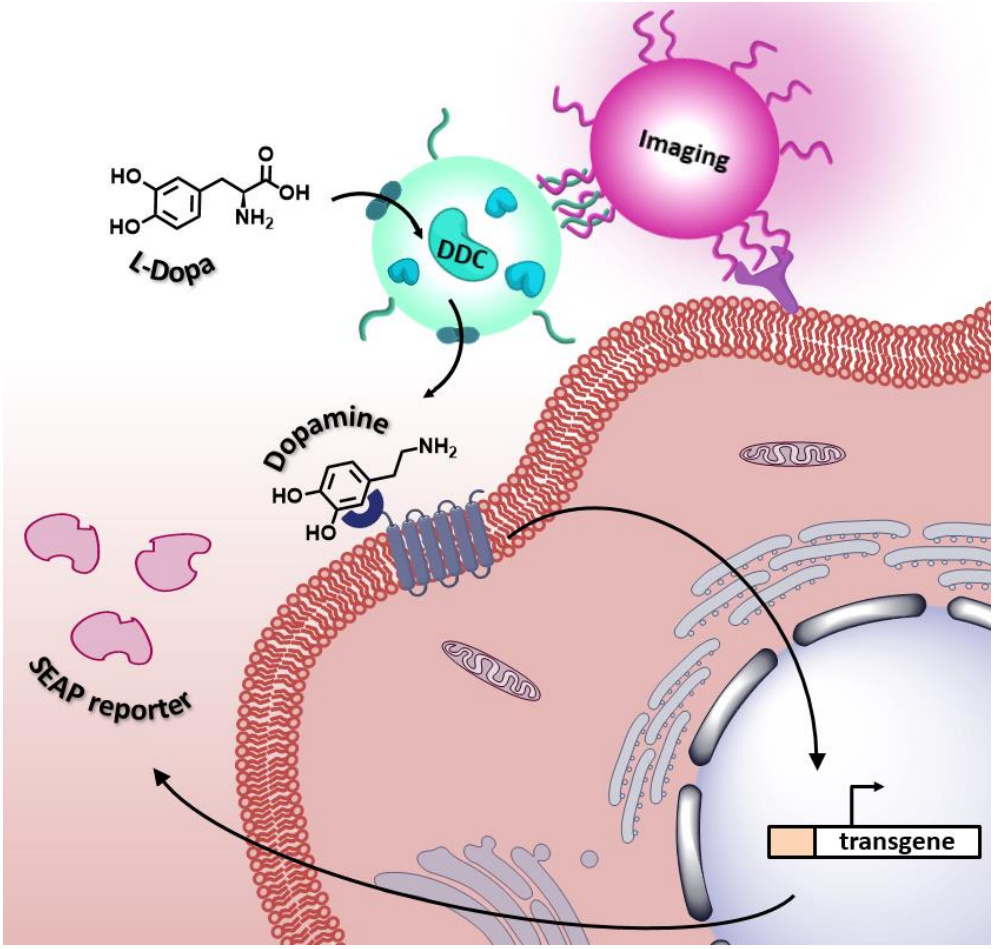

Figure 1. Schematic illustration of cell attachment of DNA-zipped theranostic polymersome clusters composed of two distinct compartments: therapeutic DDC-Ncomp and imaging Dye-Ncomp. While Dye-Ncomp contains fluorescent DY-633 dye, DDC-Ncomp contains DDC, which catalyzes the conversion of L-Dopa into dopamine. This in turn triggers gene expression in cells, resulting in the production of SEAP reporter enzyme.

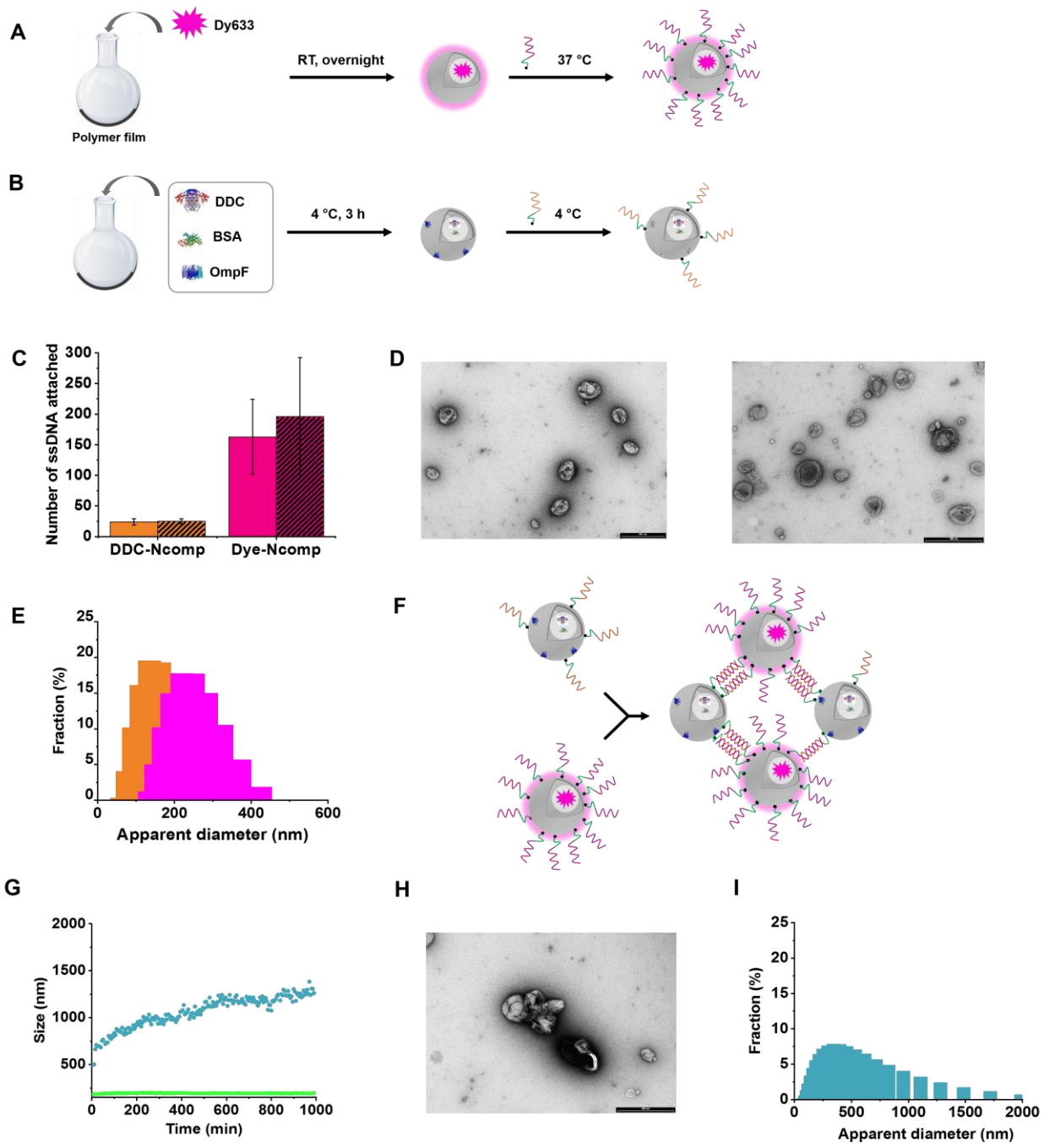

Figure 2. Design of DNA-zipped theragnostic polymersome clusters: A) Schematic representation of the formation of DDC-Ncomp linked with spacer-ssDNAa; B) Schematic representation of the formation of Dye-Ncomp linked with spacer-ssDNAb; C) Average numbers of ssDNA (solid) and spacer-ssDNA (stripped) linked to DDC-Ncomp (orange) and Dye-Ncomp (pink), as determined by FCS; D) TEM micrographs of DDC-Ncomp linked with

spacer-ssDNAa (left) and Dye-Ncomp linked with spacer-ssDNAb (right); E) Average apparent diameter of DDC-Ncomp linked with spacer-ssDNAa (orange) and Dye-Ncomp (pink) linked with spacer-ssDNAb; F) Schematic representation of the formation of theranostic cluster constituted by DDC-Ncomp and Dye-Ncomp linked together via hybridization of their complementary spacer-ssDNA; G) The change of apparent size of theranostic clusters DDC-linked by ssDNA (green) and spacer-ssDNA (blue) as a function of time; H) TEM micrograph of polymersome clusters (scale bar is 500 nm); I) Average apparent diameters of DDC-Ncomp and Dye-Ncomp polymersome clusters.

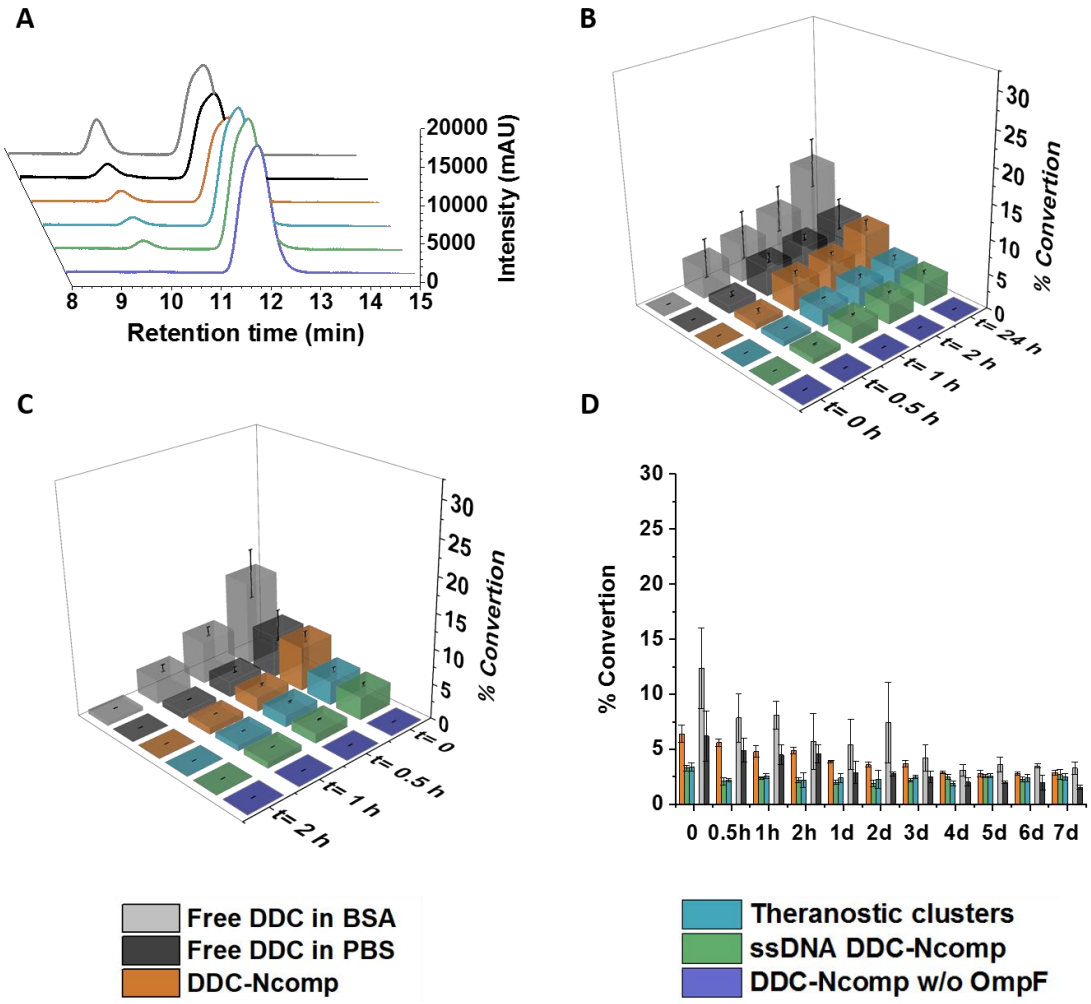

Figure 3. A) HPLC chromatograms showing elution peaks corresponding to dopamine (retention time 10.1 min) and L-Dopa (retention time 11.8 min) for free DDC in PBS (grey), free DDC in the presence of BSA (black), DDC-encapsulating polymersomes (DDC-Ncomp, orange), DDC-Ncomp theranostic clusters (blue), ssDNA-functionalized DDC-Ncomp (green) and control DDC-Ncomp without OmpF (purple), after reaction for 24 h at 37 °C. B) Processed HPLC data showing the percent conversion of L-Dopa to dopamine by the different DDC-containing samples and assemblies, illustrating the kinetics of these systems up to 24 h at 37 °C in PBS. C) Processed HPLC data showing the stability of these systems up to 2 h at 37 °C in

PBS. D) Processed HPLC data showing the stability of these systems up to 24 h at 4 °C in PBS. Full conversion (100% conversion) equates to a concentration of 490 µM dopamine.

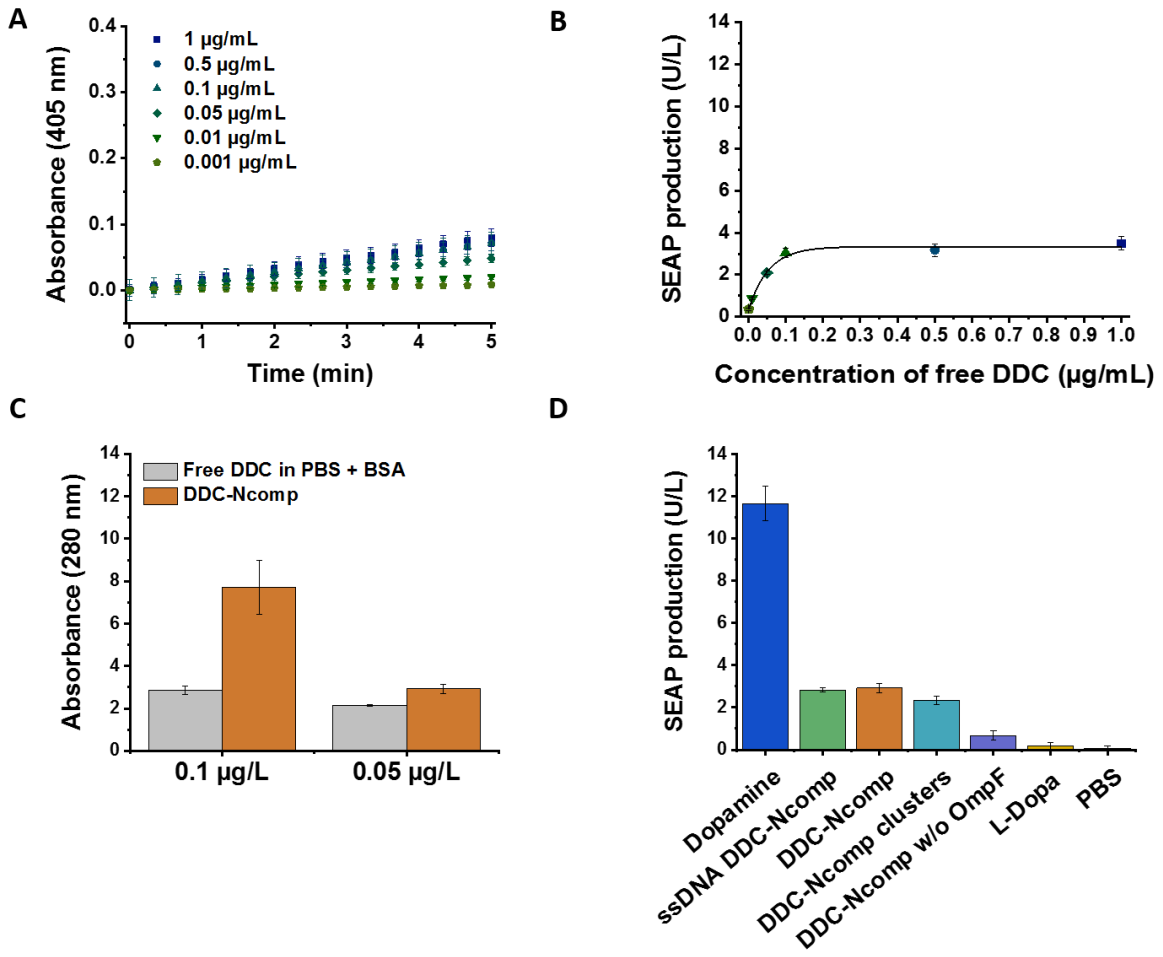

Figure 4. A) Absorbance-monitoring of the enzymatic production of chromogenic *p*-nitrophenol from SEAP substrate *p*-nitrophenyl phosphate in the cell supernatant, to assess cellular production of SEAP induced by different concentrations of free DDC (0.001 µg/mL to 1 µg/mL) in the presence of 0.1 wt% of BSA. B) Cell expression of SEAP (U/L) induced by different concentrations of free DDC (with BSA) after 3 days. C) Comparison of cellular production of SEAP (U/L) induced by DDC-encapsulating polymersomes or free DDC in BSA, at 0.1 µg/mL or 0.05 µg/mL DDC concentration. D) Cell expression of SEAP (U/L) induced by free dopamine (dark blue), ssDNA-functionalized DDC-Ncomp (green), DDC-

encapsulating polymersomes (orange), DDC-Ncomp theragnostic clusters (blue), control DDC-Ncomp without OmpF(purple), L-Dopa (grey) and PBS only (black).

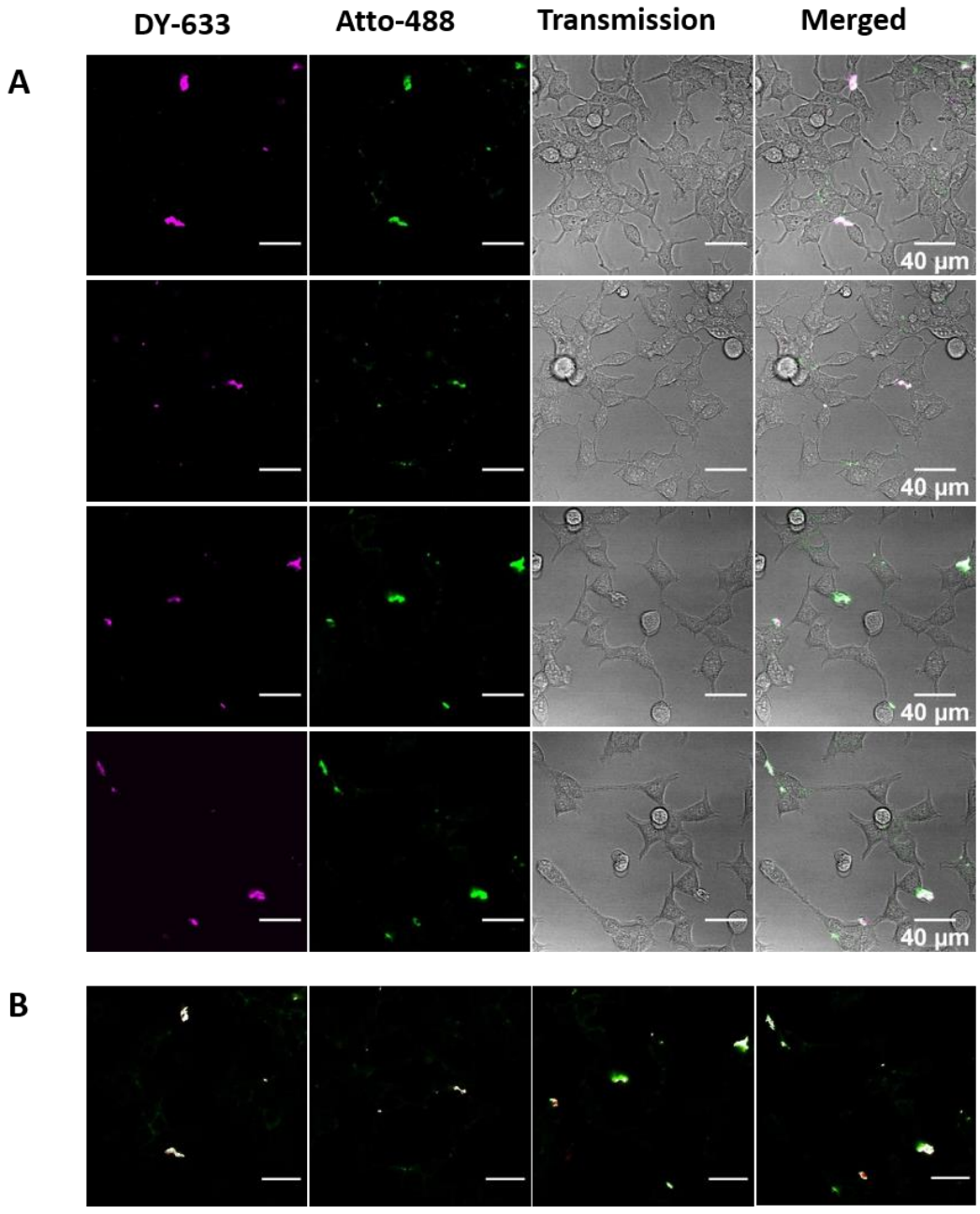

Figure 5. CLSM micrographs from four different locations of 488-633-Ncomp clusters attached to the surface of HEK_{REWARD} cells after incubation for 24 h, showing separate DY-633

and Atto-488 channels, transmission channel and merged images (scale bar = 40 μm). B) Merged DY-633 and Atto-488 channels of the four locations with colocalized regions appearing in white. Colocalization analysis of the four locations resulted in a Pearson's coefficient of 0.77 ± 0.09. Scale bar = 90 pixels or 37.8 μm

We have developed nanocompartment cluster-based nanotheranostics implementing activation of cell-membrane receptors. Polymersome clusters segregate Dopa decarboxylase (DDC) and fluorescence probes into distinct compartments. The compartment hosting DDC enables conversion of L-Dopa to dopamine, which interacts with human dopamine receptor 1 to induce a cellular response. The compartment loaded with dye allows spatiotemporal monitoring of the interaction between clusters and cells.

Nanotheranostics

*Claire E. Meyer, Juan Liu, Ioana Craciun, Dalin Wu, Hui Wang, Mingqi Xie, Martin Fussenegger, Cornelia G. Palivan**

Segregated nanocompartments containing therapeutic enzymes and imaging compounds within DNA-zipped polymersome clusters for advanced nanotheranostic platform